Ballistic-Performance Optimization of A Hybrid Carbon-Nanotube/E-Glass Reinforced Poly-Vinyl-Ester-Epoxy-Matrix Composite Armor

M. Grujicic, B. Pandurangan. D. C. Angstadt

Department of Mechanical Engineering
Clemson University, Clemson SC 29634

K. L. Koudela

Applied Research Laboratory, Pennsylvania State University
155, ARL Building, University Park, PA 16802

B. A. Cheeseman

Army Research Laboratory – Survivability Materials Branch
Aberdeen, Proving Ground, MD 21005-5069

Correspondence to:[1]
Mica Grujicic, 241 Engineering Innovation Building, Clemson, SC 29634-0921;
Phone: (864) 656-5639, Fax: (864) 656-4435, E-mail: mica.grujicic@ces.clemson.edu

ABSTRACT

The material model for a Multi-Walled Carbon Nanotube (MWCNT) reinforced poly-vinyl-ester-epoxy matrix composite material (carbon nanotube reinforced composite mats, in the following) developed in our recent work [1], has been used in the present work within a transient non-linear dynamics analysis to carry out design optimization of a hybrid polymer-matrix composite armor for the ballistic performance with respect to the impact by a Fragment Simulating Projectile (FSP). The armor is constructed from E-glass continuous-fiber poly-vinyl-ester-epoxy matrix composite laminas interlaced with the carbon nanotube reinforced composite mats. Different designs of the hybrid armor are obtained by varying the location and the thickness of the carbon nanotube reinforced composite mats.

The results obtained indicate that at a fixed thickness of the armor, both the position and the thickness of the carbon nanotube reinforced composite mats affect the

[1] **Keywords: Vinyl Ester Epoxy; Carbon Nanotubes; Composite Materials; Armor**
PACS code: 81.05.Tp (Fullerenes and related materials)

Report Documentation Page

Form Approved
OMB No. 0704-0188

1. REPORT DATE	2. REPORT TYPE	3. DATES COVERED
2007		**00-00-2007 to 00-00-2007**

4. TITLE AND SUBTITLE	5a. CONTRACT NUMBER
Ballistic-Performance Optimization of A Hybrid Carbon-Nanotube/E-Glass Reinforced Poly-Vinyl-Ester-Epoxy-Matrix Composite Armor	5b. GRANT NUMBER
	5c. PROGRAM ELEMENT NUMBER
6. AUTHOR(S)	5d. PROJECT NUMBER
	5e. TASK NUMBER
	5f. WORK UNIT NUMBER
7. PERFORMING ORGANIZATION NAME(S) AND ADDRESS(ES) **Celmson University,Department of Mechanical Engineering,Clemson,SC,29634**	8. PERFORMING ORGANIZATION REPORT NUMBER
9. SPONSORING/MONITORING AGENCY NAME(S) AND ADDRESS(ES)	10. SPONSOR/MONITOR'S ACRONYM(S)
	11. SPONSOR/MONITOR'S REPORT NUMBER(S)

12. DISTRIBUTION/AVAILABILITY STATEMENT
Approved for public release; distribution unlimited

13. SUPPLEMENTARY NOTES
Journal of Materials Science, 42, pp. 5347-5359, 2007.

14. ABSTRACT
The material model for a Multi-Walled Carbon Nanotube (MWCNT) reinforced poly-vinyl-ester-epoxy matrix composite material (carbon nanotube reinforced composite mats, in the following) developed in our recent work [1], has been used in the present work within a transient non-linear dynamics analysis to carry out design optimization of a hybrid polymer-matrix composite armor for the ballistic performance with respect to the impact by a Fragment Simulating Projectile (FSP). The armor is constructed from E-glass continuous-fiber poly-vinyl-ester-epoxy matrix composite laminas interlaced with the carbon nanotube reinforced composite mats. Different designs of the hybrid armor are obtained by varying the location and the thickness of the carbon nanotube reinforced composite mats. The results obtained indicate that at a fixed thickness of the armor, both the position and the thickness of the carbon nanotube reinforced composite mats affect the ballistic performance of the armor. Specifically, it is found that the best performance of the armor is obtained when thicker carbon nanotube reinforced composite mats are placed near the front armor face, the face which is struck by the projectile. The results obtained are rationalized using an analysis of the elastic wave reflection and transmission behavior at the lamina/met and laminate/air interfaces.

15. SUBJECT TERMS

16. SECURITY CLASSIFICATION OF:			17. LIMITATION OF ABSTRACT	18. NUMBER OF PAGES	19a. NAME OF RESPONSIBLE PERSON
a. REPORT **unclassified**	b. ABSTRACT **unclassified**	c. THIS PAGE **unclassified**	**Same as Report (SAR)**	**38**	

ballistic performance of the armor. Specifically, it is found that the best performance of the armor is obtained when thicker carbon nanotube reinforced composite mats are placed near the front armor face, the face which is struck by the projectile. The results obtained are rationalized using an analysis of the elastic wave reflection and transmission behavior at the lamina/met and laminate/air interfaces.

I. INTRODUCTION

Owing their high strength- and stiffness-to-weight ratios, polymer-matrix composites are increasingly being used as structural materials in the construction of rapidly deployable armored vehicles whose primary role is the support of ground troops. In addition, polymer-matrix composites are being used as (lightweight) armor in the same vehicles. This is particularly evidenced in the case of the M1114 High Mobility Multi-purpose Wheeled Vehicles (HMMWVs or more commonly referred to as the *Humvees*) in which the ballistic protection is attained through the use of a phenolic-matrix composite armor system generally known as the *HJ1*. This patented, licensed composite material system is compliant with the MIL-L-64154 U.S. Military Department of Defense Specifications [2] and is comprised of high-strength S-2 glass-fiber reinforcements laminated into phenolic-matrix hard-armor panels.

Recent experiences of the U.S. military forces in Iraq clearly established the tradeoffs between various armor protection concepts for battle military vehicles. In general, the battlefield demands light, maneuverable and fast vehicles which, at the same time, can provide an adequate level of protection for the vehicle occupants. Traditional steel armor while being able to provide the required protection for the on-board personnel and do it at a relatively low cost, contributes a prohibitively large additional weight to the battle vehicles, often increasing the loads beyond the levels anticipated during the vehicle design [3]. Consequently, the vehicles tend to break down at an unacceptably high rate due to failure in the engine, transmission, suspension and/or braking systems. In addition, the fuel efficiency of the vehicles is seriously compromised, as is their ability to carry additional personnel in the case of emergency. Furthermore, reduced mobility of the steel-armor protected battle vehicles

makes them an easier target to enemy fire. Due to the aforementioned shortcomings of the steel armor, the military vehicles are increasingly being protected using advanced fiber-reinforced polymer-matrix composite armor systems. While the use of the fiber-reinforced polymer-matrix composite armor is beneficial with regard to attaining a lower vehicle weight, higher vehicle maneuverability, higher fuel efficiency, lower load levels imposed on the vehicle power train, suspension and breaking systems, the associated level of protection of the on-board personnel and the cost of the armor remain outstanding issues.

With respect to their overall performance under ballistic impact conditions, advanced fiber-reinforced polymer-matrix composites are generally classified into two main categories [4]: (a) High-strength/ high-stiffness composites (typically based on carbon-fiber reinforcements), which are highly effective in deforming and/or fracturing the incoming projectile while having a very limited ability for absorbing the projectile's kinetic energy; and (b) High-ductility/high-toughness advanced composites (typically based on glass or aramid reinforcements) whose properties are optimized with respect to absorbing the maximum fraction of the kinetic energy carried by the projectile. It has been recently suggested that polymer-matrix composites reinforced with carbon nanotubes may combine the benefits offered by the two aforementioned classes of advanced fiber-reinforced polymer-matrix composite armors [5]. That is, due to a high hardness of the nanotubes, carbon-nanotube reinforced polymer-matrix composite armor may be very effective in eroding/fracturing the projectile while a high strength combined with a high ductility of these composite materials makes them very efficient in absorbing the projectile's kinetic energy.

Due to their exceptional mechanical properties, a high aspect ratio and a low density, single-walled carbon nanotubes (SWCNTs) and multi-walled carbon nanotubes (MWCNTs) have been perceived as ideal mechanical reinforcement candidates for the next generation of polymer-based composites [6]. An elastic modulus as high as 1TPa and a tensile strength close to 60GPa have been reported in SWCNTs. These values are five and at least thirty times greater than their respective counterparts in steels, and at only one sixth of the weight [7-10]. Thus, the SWCNTs appear to be ideal mechanical

reinforcements for lightweight composite systems. However, the material and the processing cost for the SWCNTs, even when they are produced using large-scale high-yield technologies, are very high primarily due to the costly separation and non destructive purification processing. Consequently, while the mechanical properties of MWCNTs are generally less attractive (the elastic modulus typically around 350GPa and a tensile strength around 8GPa, [7]) relative to those found in the SWCNTs, the lower-cost MWCNTs are currently being considered as a more realistic mechanical reinforcement candidate for the commercially-viable polymer-matrix composites.

A number of experimental investigations reported in the literature established that the mechanical properties of both SWCNT- and MWCNT-reinforced polymer-matrix composites are significantly below their theoretically predicted potential [e.g. 11] and that they are controlled by the extent of dispersion of the nanotubes in the polymer matrix and by the nanotube/polymer interface bond strength [11-14]. The nanotube reinforcements are often found aggregated into bundles (ropes), weakly interacting via the van der Waals attractive forces [15,16]. Such bundles can contain up to several hundred nanotubes arranged in a hexagonal lattice [15-17]. The nanotubes within a bundle can easily slide relative to each other giving rise to a low value of the shear modulus of the carbon nanotube bundles [17]. As an example, the elastic modulus of the microscopic polymer-free SWCNT-based fibers and strands are found to be only 80GPa [18] and 77GPa [19], respectively. In addition to reducing the shear modulus, the nanotube aggregation gives rise to the undesirable reduction in the reinforcement aspect ratio. As reviewed in our recent work [5], obtaining a homogeneous dispersion of the nanotubes in the polymer matrix is not easily accomplished primary because of very low solubility of the nanotube bundles in most solvents and a number of approaches are being pursued in order to overcome this problem. As far as the nanotube/polymer interfacial-bonding strength is concerned, its magnitude is believed to be limited by the atomically-smooth, non-reactive nature of the nanotubes outer wall [6]. This, in turn, limits the load transfer from the polymer matrix to nanotubes which controls the extent of stiffening/strengthening induced by the nanotube reinforcements. As discussed in our recent work [5], several strategies for

synthesis of the nanotube-reinforced polymer-matrix composites with improved reinforcement/matrix bonding have been developed. Several of the aforementioned efforts and approaches have resulted in significant improvements of the homogeneity of nanotubes distribution within the polymer matrix and of the nanotube/polymer interfacial bond strength.

In our ongoing/future work [20] (the present paper is a part of the ongoing/future work), a new class of MWCNT-reinforced poly-vinyl-ester-epoxy based armor for mitigation of the effects of Improvised Explosive Devices (IEDs) is being developed. For such armor, a good load transfer between the polymer matrix and the nanotube reinforcements is important for its structural (static load-bearing) performance and a tendency for interfacial failure and the associated reinforcement pull-out are crucial for its energy-absorbing ballistic performance. Toward that end, the reinforcement/polymer interfaces are carefully engineered by combining the polymer wrapping technique [e.g. 21] with a covalent-type functionalization of the MWCNT sidewall [e.g. 22].

The objective of the present work is to carry out the design optimization analysis of a hybrid armor constructed from E-glass continuous-fiber poly-vinyl-ester-epoxy matrix composite laminas interlaced with the carbon nanotube reinforced composite mats. The mats have been produced in our ongoing/future work [20] through a combination of nanotube-reinforced fiber spinning and fiber lay-out techniques while the hybrid-armor laminates will be produced using the standard Vacuum Assisted Resin Transfer Molding (VARTM) process. The objective of the design optimization is an improvement in the ballistic performance of the armor with respect to the IEDs. The analysis involves transient non-linear dynamics calculations of the fragment/armor impact and the use of the material model for a MWCNT-reinforced poly-vinyl-ester-epoxy matrix composite developed in our recent work [1] along with the available materials models for the E-glass continuous-fiber poly-vinyl-ester-epoxy matrix composite laminas and the AISI 4340 steel fragment. Different designs of the hybrid armor are obtained by varying the location and the thickness of the carbon nanotube reinforced composite mats. The results of the present work will be used to guide the

design of the hybrid armor which will be fabricated and tested for ballistic performance in our ongoing/future work [20].

The organization of the paper is as follows. A brief overview of the non-linear dynamics computational procedure utilized in the present work is given in Section II.1. Constitutive models used to represent the behavior of the projectile and the armor materials under ballistic impact conditions are discussed in Section II.2. Details of the numerical model used to analyze the impact and penetration of the armor by a fragment simulating projectile are presented in Section II.3. The results obtained in the present work are presented and discussed in Section III. The main conclusions resulting from the present work are summarized in Section IV.

II. COMPUTATIONAL PROCEDURE

II.1 Non-linear Dynamics Modeling of High-rate Phenomena

All the calculations carried out in the present work are done using AUTODYN, a general purpose non-linear transient dynamics modeling and simulation software [23]. Within AUTODYN, the appropriate mass, momentum and energy conservation equations coupled with the materials modeling equations and subjected to the appropriate initial and boundary conditions are solved. The numerical methods used for the solution of these equations involve finite difference, finite volume and finite element methods and the choice of the method (i.e. of the "*processor*" as referred to in AUTODYN) used depends on the physical nature of the problem being studied. For multi-domain problems, different domains can be analyzed using different processors such as the Lagrange processor or the SPH (Smooth Particle Hydrodynamics) processor (typically used for bulk solid-continuum structures), the Euler processor (commonly used for modeling gases, liquids or solids subject to large deformations) and the Shell processor (designated for modeling thin-walled solid structures).

In the present work, the ballistic performance of a hybrid polymer-matrix composite armor under FSP (Fragment Simulating Projectile) threats is analyzed using the Lagrange processor. The interactions between different sub-domains are accounted for through the use of the sub-domain interaction options within AUTODYN [23]. A

detailed overview of the sub-domain interaction options can be found in our recent work [24]. Also, the effect of the processor choice (Lagrange vs. SPH) on the computational results can be found in Ref. [24].

II.2 Material Constitutive Models

As discussed in the previous section, for the boundary value problems analyzed by AUTODYN to be fully specified, material-specific constitutive relations between the flow variables (pressure, mass density, internal energy density, temperature, etc.) have to be defined. These additional relations typically involve an equation of state, a strength equation and a failure equation for each constituent material. These equations arise from the fact that, in general, the total stress tensor can be decomposed into a sum of a hydrostatic stress (pressure) tensor (which causes a change in the volume/density of the material) and a deviatoric stress tensor (which is responsible for the shape change of the material). An equation of state then is used to define the corresponding functional relationship between pressure, mass-density (specific volume) and internal energy density (temperature), while a strength relation is used to define the appropriate equivalent plastic-strain, equivalent plastic-strain rate, and temperature dependencies of the yield surface (a scalar function of the deviatoric stress or total stress components). In addition, a material model generally includes a failure criterion, i.e. an equation describing the (hydrostatic or deviatoric) stress and/or strain condition which, when attained, causes the material to fracture and lose (abruptly, in the case of brittle materials or gradually, in the case of ductile materials) its ability to support normal and shear stresses.

In the following, a brief description is given of the models for the materials utilized in the present work, i.e. for AISI 4340 Steel (FSP), E-Glass continuous-fiber-reinforced-poly-vinyl-ester-epoxy (major portion of the hybrid composite armor) and MWCNT-reinforced poly-vinyl-ester-epoxy composite mats (strategically placed within the hybrid composite armor). The values of the material parameters for AISI 4340 Steel, defined in the remainder of the section, are available in the AUTODYN materials library [23]. The data cannot be disclosed here due to copyright violation concerns. The corresponding material parameters for E-Glass continuous-fiber-reinforced-poly-

vinyl-ester-epoxy and MWCNT-reinforced poly-vinyl-ester-epoxy composite mats can be found in our previous work [1].

II.2.1 AISI 4340 Steel

Equation of State

For AISI 4340 Steel, a linear type of equation of state is used which assumes a Hooke's law type relationship between the pressure, P, and the relative density change $\mu = \left(\frac{\rho}{\rho_0} - 1 \right)$ as:

$$P = K\mu \tag{1}$$

where ρ is density, K is the bulk modulus of the material and the subscript o is used to denote the initial material state.

Strength Model

To represent the constitutive response of AISI 4340 Steel under deviatoric stress, the Johnson-Cook model [25] is used. This model is capable of representing the material behavior displayed under large-strain, high deformation rate, high-temperature conditions, of the type encountered in problems dealing with hypervelocity impact and penetration conditions. Within the Johnson-Cook model, the yield stress is defined as:

$$Y = \left[A_1 + B_1 \varepsilon_{pl}^{n} \right] \left[1 + C_1 \log \dot{\varepsilon}_{pl} \right] \left[1 - T_{H0}^{m} \right] \tag{2}$$

where ε_{pl} is the equivalent plastic strain, $\dot{\varepsilon}_{pl}$ the equivalent plastic strain rate, A_1 the zero plastic strain, unit plastic strain rate, room temperature yield stress, B_1 the strain hardening constant, n the strain hardening exponent, C_1 the strain rate constant, m the thermal softening exponent and $T_{H0} = (T - T_{room})/(T_{melt} - T_{room})$ a room temperature (T_{room}) based homologous temperature while T_{melt} is the melting temperature. All temperatures are given in Kelvin.

Failure Model

For AISI 4340 Steel which fails predominantly in a ductile mode, the failure condition is defined using the Johnson-Cook failure model [25]. The progress of failure according to the Johnson-Cook failure model is defined by the following cumulative damage law:

$$D = \sum \frac{\Delta \varepsilon}{\varepsilon_f} \tag{3}$$

where $\Delta\varepsilon$ is the increment in effective plastic strain with an increment in loading and ε_f, is the failure strain at the current state of loading which is a function of the mean stress, the effective stress, the strain rate and the homologous temperature, given by:

$$\varepsilon_f = \left[D_1 + D_2 \exp(D_5 \sigma^*)\right]\left[1 + D_4 \ln \dot{\varepsilon}_{pl}\right]\left[1 + D_5 T_{H0}^m\right] \tag{4}$$

where σ^* is mean stress normalized by the effective stress. The parameters D_1, D_2, D_3, D_4 and D_5 are all material specific constants. Failure is assumed to occur when D=1.

Erosion Model

When the Lagrange solver is used for computations, numerical difficulties arising from excessive distortion of the cells are often overcome by using an erosion algorithm, which at a predefined level of equivalent geometrical or plastic strain removes excessively distorted cells while transferring the momentum associated with the removed nodes to the remaining nodes. An erosion criterion corresponding to a value of 2.00 for the instantaneous geometrical strain is used in the present work for the AISI 4340 Steel FSP.

II.2.2 Fiber-reinforced Polymer-matrix Composite Laminates

The mechanical behavior of composite laminates is generally more complex than that found in metals or ceramics. As discussed in our previous work [4], this increased complexity of the composite laminates can be attributed to a number of phenomena, such as: (a) anisotropy of the material stiffness properties; (b) anisotropy in the failure strength and in the post-failure behavior; (c) coupling between the hydrostatic and deviatoric (stress and strain) quantities; (d) non-linearity in pressure vs. density relation; and (e) onset of compaction when the material contains porosity.

In the present work, the mechanical response of both the E-glass reinforced poly-vinyl-ester-epoxy matrix composite laminates and the MWCNT-reinforced poly-vinyl-ester-epoxy mats under large deformation and high deformation-rate conditions (which are encountered during ballistic testing) are represented using the ballistic orthotropic material model developed by Clegg et al. [26]. This model is based on the original ideas proposed by Anderson et al. [27] for coupling material's anisotropy with the non-linear material response. Since this model was reviewed in detail in our recent work [28], it will be only summarized here. As stated earlier, all the material parameters for the E-glass reinforced poly-vinyl-ester-epoxy matrix composite laminates and the MWCNT-reinforced poly-vinyl-ester-epoxy mats can be found in our previous work [1].

A composite armor panel is typically constructed by laminating few dozens of individual plies (laminas) so that the overall in-plane properties of the laminate are isotropic. Therefore, composite laminates are classified as *"transversely isotropic"* materials. Furthermore, as established in our previous work [1], the MWCNT-reinforced poly-vinyl-ester-epoxy mats contain a random in-plane distribution of MWCNTs and, hence, can also be considered as a transversely isotropic material.

Equation of State

Using the following definition for the pressure, $P = -\frac{1}{3}(\sigma_{11} + \sigma_{22} + \sigma_{33})$**, the following definition for the volumetric strain,** $\varepsilon_{vol} = \varepsilon_{11} + \varepsilon_{22} + \varepsilon_{33}$ **and the linear elastic stress-strain relation for a transversely-isotropic material, the equation of state can be written as:**

$$P = -\frac{1}{9}\left[\bar{c}_{11} + \bar{c}_{11} + \bar{c}_{33} + 2(\bar{c}_{11} + \bar{c}_{13} + \bar{c}_{13})\right]\varepsilon_{vol} - \frac{1}{3}(\bar{c}_{11} + \bar{c}_{11} + \bar{c}_{13})\varepsilon_{11}^{d} - \frac{1}{3}(\bar{c}_{11} + \bar{c}_{11} + \bar{c}_{13})\varepsilon_{11}^{d} - \frac{1}{3}(\bar{c}_{13} + \bar{c}_{13} + \bar{c}_{33})\varepsilon_{33}^{d} - (\bar{c}_{16} + \bar{c}_{26} + \bar{c}_{36})\varepsilon_{11} \quad \textbf{(5)}$$

Where σ_{ij}**'s are the stress components,** c_{ij}**'s are the elastic-stiffness coefficients and** ε_{ij}^{d} **are the components of the deviatoric strain. It should be noted that *"principal"* direction *3* is taken to coincide with the armor through-the-thickness direction while**

principal directions *1* and *2* are the in-plane directions.

The first term on the right hand side of Eq. (5) represents the standard linear relationship between the pressure and volumetric strain while the remaining terms on the right hand side of the same equation account for the coupling between the pressure and the deviatoric strain. The later terms of Eq. (5) are absent in the case of isotropic materials. The constant part of the first term on the right hand side of Eq. (5) represents the effective bulk modulus of the material, K. Under high strain-rate ballistic loading conditions, the relationship between the pressure and the volumetric strain is typically non-linear and, consequently, the first term on the right hand side of Eq. (5) is replaced by a non-linear relationship between the pressure and volumetric strain. In the present work, the Mie-Gruneisen [29] equation of state is used to represent the first term on the right hand side of Eq. (5).

The Mie-Gruneisen equation of state defines the effect of current material mass density, ρ, and internal energy density, e, on pressure, P, as:

$$P = P_H + \Gamma\rho\left[e - e_H\right] \tag{6}$$

where the reference material states denoted by a subscript H correspond to the Hugoniot shock states of the material. These reference states are obtained by solving a system of simultaneous algebraic equations defining, for a stationary shock, the mass conservation, the momentum conservation and the energy conservation and a linear relationship between the shock speed, u_s and the particle velocity u_p. The parameter Γ appearing in Eq. (6) (the Gruneisen Gamma) is a known thermodynamic material property and is defined as $\Gamma(v) \equiv \frac{1}{\rho}\left[\frac{\partial P}{\partial e}\right]_\rho$.

Strength Model

The strength model for transversely-isotropic materials is typically represented using the following type of total-stress based six-parameter quadratic yield function:

$$f(\sigma_{ij}) = a_{11}\sigma_{11}^2 + a_{11}\sigma_{22}^2 + a_{33}\sigma_{33}^2 + 2a_{11}\sigma_{11}\sigma_{22} + 2a_{13}\sigma_{11}\sigma_{33} + 2a_{13}\sigma_{11}\sigma_{33} + 2a_{44}\sigma_{23}^2 + 2a_{55}\sigma_{31}^2 + 2a_{66}\sigma_{12}^2 = r \tag{7}$$

where a_{ij} and r are material parameters. The parameter r represents the current material's resistance towards plastic deformation and in the case of strain-hardening materials like composite laminates increases with an increase in the equivalent plastic strain.

Equation (7) is used in the following fashion:

When the middle term in Eq. (7) is less than r, no plastic deformation takes place. Otherwise, plasticity takes place. For strain-hardening materials, the value of the r parameter is increased and the stress components decreased until the equality defined by Eq. (7) is satisfied. Plastic deformation in composite laminates is assumed to take place in accordance with the "*associated*" flow rule, i.e. the magnitude of the components of the plastic strain increment scale linearly with the associated components of the stress gradient of the yield function as:

$$d\varepsilon_{ij}^{p} = d\lambda \frac{\partial f}{\partial \sigma_{ij}} \tag{8}$$

where $d\lambda$ is the plastic strain-rate multiplier.

Failure Model

The failure model for transversely-isotropic composite laminates used in the present work combines a failure initiation model with a material mechanical degradation model. Final failure is taken to occur when the material loses its ability to support any shear and/or tensile loads. The failure initiation model defines a stress or strain based criterion which when met leads to the onset of mechanical degradation of the material. Once failure is initiated, the strength and stiffness properties of the material are continuously updated in accordance with the extent of current level of material degradation. The material mechanical degradation model is based on the concept of "*cracked strain*", ε_{cr}, which as it increases from the moment of failure initiation, gives rise to a progressive increase in the extent of material damage. The maximum value of each component of cracked strain is obtained using the computed or measured values of the associated failure stress and fracture energy. The fracture energies are determined experimentally using the double cantilever beam test [30].

Once the material has failed in a particular direction the stress in that direction is set to zero while the stresses in the other directions are modified in accordance with the loss of Poisson's effect. When the failure occurs due to excessive tensile strains in the laminate through-the-thickness direction or due to excessive inter-lamellar shear strains, it is referred to as "*delamination***". On the other hand, laminate in-plane tensile stresses lead to "***reinforcement***" failure. When the material fails in more than one direction (***the bulk failure***) its properties are set to those of an equivalent isotropic material, and all tensile stresses are set to zero, while the shear stresses are set to a predefined residual shear stress level.**

In addition to the stress/strain based failure criterion described above, matrix melting and/or fiber degradation due to excessive heating can also lead to material failure. Matrix melting and the subsequent delamination failure occur when the temperature exceeds the melting point of the polymer matrix. Fiber degradation occurs when the matrix temperature exceeds a predefined fiber degradation temperature and leads to a bulk mode of failure which leaves the material only with an ability to support compressive type of stresses.

Erosion Model

The same erosion model was used as in the case of AISI 4340 Steel.

II.3 Problem Definition and Computational Analysis

In the present work, a transient non-linear dynamics analysis of the impact and penetration of a hybrid polymer-matrix composite armor (constructed from E-glass continuous-fiber poly-vinyl-ester-epoxy matrix composite laminas interlaced with MWCNT reinforced poly-vinyl-ester-epoxy composite mats) by a Fragment Simulating Projectile (FSP) is carried out in order to determine the ballistic performance and the protection potential of the armor. The work was limited to the case of a normal impact of the armor by the FSP and, due to the axisymmetric nature of the problem, all the calculations are carried out using a two-dimensional (axisymmetric) model. A simple schematic of the projectile/armor impact/penetration problem analyzed here is given in Figure 1. The projectile is cylindrical in shape with a diameter of 6.35mm and a height

of 6.35mm. A constant initial normal velocity of 609.6m/s (2000 ft/s) is assigned to the projectile made of AISI 4340 steel and thus the initial kinetic energy of the projectile is approximately 0.56kJ. A fixed thickness of 12.7mm and a fixed lateral dimension of 100mm for the armor are used for all the cases analyzed. Eight different configurations of the armor are analyzed (Figure 2). Various configurations of the armor differ with respect to the number and the location of the 50 micron thick carbon nanotube reinforced composite mats. For brevity, an abridged designation is assigned to each armor. The letters *T* (Top), *M* (Middle) and *B* (Bottom) are used respectively to denote the position of the carbon nanotube reinforced composite mats within the hybrid armor. The "*Top*" position refers to the one closest to the surface of the armor struck by the FSP. Numbers 1 and 2 are used to denote the number of 50 micron-thick carbon nanotube reinforced composite mats at a given position in the armor. The all E-glass continuous-fiber reinforced poly-vinyl-ester-epoxy matrix armor is denoted with the letter *R* (reference).

The interaction between the projectile and the armor is accounted for using the part-coupling option available in AUTODYN [4]. Except for the projectile/armor contact surfaces, zero-stress boundary conditions are prescribed on all faces of the projectile and the armor. The Lagrange processor is used to represent both the FSP and the armor. The projectile was analyzed using a mesh consisting of 800 rectangular cells, while the armor is analyzed using a mesh consisting of 6000 rectangular cells. To improve the accuracy of the analysis, smaller cells are used in the regions of the projectile and the armor involved in the projectile/armor interactions as well as in the regions inside and in the vicinity of the MWCNT-reinforced poly-vinyl-ester-epoxy matrix composite mats. A standard mesh sensitivity analysis is carried out in order to ensure that the results obtained are effectively insensitive to the size of the cells used.

III. RESULTS AND DISCUSSION

III.1 Validation of the Material Model for E-glass Reinforced Poly-vinyl-ester-epoxy Matrix Composite

Since the E-glass continuous-fiber reinforced poly-vinyl-ester-epoxy matrix composite laminas constitute the major portion of the hybrid armor analyzed in the present work, it is critical to validate its material model before assessing the potential benefits obtained through their interlacing with MWCNT reinforced poly-vinyl-ester-epoxy mats. This validation is carried out in the present section.

In our ongoing/future work [20], it was determined experimentally that the V50 velocity (the velocity at which the projectile has 50% probability of penetrating the armor) for a 25.4mm-thick E-glass continuous-fiber reinforced poly-vinyl-ester-epoxy matrix armor impacted by a 0.50 caliber (12.7mm diameter and 12.7mm high) AISI 4340 steel FSP is around 605 m/s. The results of a transient non-linear dynamics analysis carried out in the present work and displayed in Figure 3 show that 605 m/s is a good estimate for the V50. That is, at a velocity of 600 m/s the 0.50 caliber FSP does not penetrate the 25.4mm-thick E-glass continuous-fiber reinforced poly-vinyl-ester-epoxy matrix armor, while at a velocity of 610 m/s the armor is penetrated and the FSP's residual velocity is around 120 m/s.

In passing, it should be noted that the velocity vs. time curves shown in Figure 3 are not very monotonic but show periodic more pronounced drops in the projectile velocity, as labeled with A and B, in this figure. These events correspond to the arrival of compression waves (generated at the FSP/armor interface) to the back face of the projectile. Such waves are reflected as rarefaction waves at the back face of the FSP and continue to travel towards the FSP/armor interface where they are attenuated and reflected, as compression waves, back into the projectile. This process continues until the waves die out.

Figure 4(a) shows the 0.50 caliber FSP initially propelled at a velocity of 605 m/s which was defeated after a partial penetration obtained experimentally in our ongoing/future work [20]. The corresponding FSP/armor configuration obtained computationally in the present work is displayed in Figure 4(b). A comparison of Figures 4(a) and 4(b) suggests a close agreement between the observed and calculated depths of penetration, the observed and calculated extents of armor delamination and between the observed and calculated FSP deformed shapes.

Based on the discussion presented above in conjunction with Figures 3 and 4 it appears justified to conclude that the present model for the E-glass continuous-fiber reinforced poly-vinyl-ester-epoxy matrix armor can reasonably well account for the ballistic performance of this material when impacted with the FSP.

III.2 The Effect of Hybrid-Armor Interlacing with MWCNT-reinforced Poly-Vinyl-Ester Epoxy Mats

In our ongoing experimental work [20], hybrid armor laminates based on the E-glass continuous-fiber reinforced poly-vinyl-ester-epoxy laminas interlaced with the MWCNT-reinforced poly-vinyl-ester epoxy mats are being fabricated and will be ultimately tested for ballistic performance with respect to the impact of an FSP. To reduce the material cost, 12.7 mm-thick armor laminates are being fabricated. Consequently, a smaller 0.30 caliber (7.62 mm in diameter and 7.62 mm in height) FSP is used. The results of the transient non-linear dynamics computational analysis carried out in the present work are displayed in Figures 5(a)-(b). It should be recalled that the all E-glass continuous-fiber reinforced poly-vinyl-ester-epoxy matrix armor is denoted with the letter *R*. The results displayed in Figure 5(a) correspond to the armors in which 50μm-thick MWCNT-reinforced poly-vinyl-ester epoxy mats were used while the results displayed in Figure 5(b) correspond to the armors in which single 100μm-thick MWCNT-reinforced poly-vinyl-ester epoxy mats were used. The results displayed in Figures 5(a)-(b) can be summarized as follows:

(a) In the case of the armor based on 50μm-thick MWCNT-reinforced poly-vinyl-ester-epoxy matrix mats, Figure 5(a), only the 1T_1M and 1T_1M_1B designs show a superior ballistic performance (i.e. a lower residual velocity of the projectile) relative to the all E-glass continuous fiber-reinforced poly-vinyl-ester-epoxy composite armor (*R*);

(b) The presence of MWCNT-reinforced poly-vinyl-ester-epoxy matrix mats in the bottom location compromises the ballistic performance of the armor. That is, the exit FSP velocity in the case of the 1T_1M_1B armor is increased relative to the 1T_1M armor;

(c) No major changes on the extent of monotony of the velocity vs. time curves in the hybrid armor relative to the all E-glass continuous fiber-reinforced poly-vinyl-ester-epoxy composite armor (R) can be observed. These results are consistent with the fact that the acoustic impedance of the E-glass continuous fiber-reinforced poly-vinyl-ester-epoxy laminas and the MWCNT-reinforced poly-vinyl-ester-epoxy matrix mats differ only by 5-6% so that only a small fraction of the energy carried by the compression waves is reflected at the lamina/mat interfaces;

(d) No observable erosion/fracturing of the FSP is observed (the results not shown for brevity), so that the effect of interlacing the E-glass continuous fiber-reinforced poly-vinyl-ester-epoxy with the MWCNT-reinforced poly-vinyl-ester-epoxy matrix mats is mainly the result of the increased ability of the armor to attenuate the projectile's kinetic energy;

(e) In the case of the hybrid armor interlaced with a single 100μm-thick MWCNT-reinforced poly-vinyl-ester-epoxy matrix mat, all the armor designs outperform the all E-glass continuous fiber-reinforced poly-vinyl-ester-epoxy composite armor;

(f) The placement of the MWCNT-reinforced poly-vinyl-ester-epoxy matrix mats at the top position still yields the best ballistic armor performance of the armor while the bottom position appears to be least desirable; and

(g) Points (c) and (d) concerning the results displayed in Figure 5(a) also apply in the case of the results displayed in Figure 5(b).

To help reveal the possible reasons behind the observed effect of the location of the MWCNT-reinforced poly-vinyl-ester-epoxy composite mats on the ballistic performance of the armor, a material deformation/failure status plot is given in Figure 6 for the 2_T (the overall best) armor design and the 2_B armor design (the worst among the ones interlaced with a single 100μm-thick MWCNT-reinforced poly-vinyl-ester-epoxy matrix composite mat). The results displayed in Figure 6 show that while there is no significant difference in the extent of armor delamination in the two armors and that the 2_B armor tend to suffer from a plug-type failure which is associated with a lower extent of energy absorption.

III.3 Statistical Sensitivity Analysis

The results presented in the previous section established that the optimum placement of the MWCNT-reinforced poly-vinyl-ester-epoxy matrix mats is in the upper portion of the armor. It should be noted that there was a considerable variance associated with the material parameters of MWCNT-reinforced poly-vinyl-ester-epoxy matrix mats as determined in our previous work [1]. It is, hence, critical to assess the sensitivity of the results obtained in the previous sections with respect to the established uncertainty in the material model parameters. Toward that end, a sensitivity analysis for the optimal 2_T design of the hybrid armor is carried out in the present section.

Within the context of statistical analysis, the term factors, is used to denote the parameters whose uncertainty is analyzed. To determine the sensitivity of the optimum design with respect to variations in the factors (material model parameters in the present case), the method commonly referred to as the statistical sensitivity analysis [31] will be used in the present work.

The first step in the statistical sensitivity analysis is to identify the factors and their ranges of variation. In the case of the material model for the MWCNT-reinforced poly-vinyl-ester-epoxy matrix mats, there is a large number of potential factors (five elastic constants, six parabolic yield function coefficients, four failure initiation stresses, four fracture energies, etc., all for a transversely isotropic material). A comprehensive statistical sensitivity analysis which would include the effect of all these factors is beyond the scope of the present work. Instead each set of material parameters is defined as a single factor. For example, all the elastic stiffness coefficients are considered as a single factor. Four factors (stiffness, strength, failure initiation stresses and fracture toughness) are used in the present work.

Typically, two to four values (generally referred to as "*levels*") should be selected for each factor. In the present case, three values are associated with each factor. One level of the factors (assigned a value of 1) corresponds to the values of the material parameters used in Section III.2. The other two levels of the factors correspond to the values of the material parameters increased or decreased by one standard deviation for all materials parameters associated with a given factor. Therefore, the values of each

parameter associated with a given factor and corresponding to a given level of that factor is obtained by multiplying the value of the level with the magnitude of the parameters as used in the previous section. A list of the four factors used in the present work and their levels is given in Table 1. Level 2 corresponds to the values of the material model parameters used in Section III.2.

The next step in the statistical sensitivity analysis is to identify the (experimental or computational) procedures (the transient non-linear dynamics analysis in the present work) which need to be performed in order to quantify the effect of the selected factors. In general, a factorial design approach can be used to determine the total number of analyses that have to be carried out. Within such an approach, all possible combinations of the factor levels are used. However, the number of the analyses to be carried out can quickly become unacceptably large as the number of factors and levels increases. In the present case, 81 ($=3^4$) analyses have to be performed according to the full factorial approach. To overcome this problem, i.e. to reduce the number of analyses which needs to be performed, the orthogonal matrix method [32] will be used. The orthogonal matrix method contains a column for each factor, while each row represents a particular combination of the levels for each factor to be used in the analyses. Thus, the number of analyses which needs to be performed is equal to the number of rows of the corresponding orthogonal matrix. The columns of the matrix are mutually orthogonal, that is, for any pair of columns, all combinations of the levels of the two associated factors appear and each combination appears an equal number of times. A limited number of standard orthogonal matrices [33] is available to accommodate specific numbers of the factors with various numbers of levels per factor. In the present work, the L_{18} 3^4 orthogonal matrix is used which defines 18 computational analyses which have to be performed. The factor levels associated with each of these analyses is given in Table 2.

A computational transient non-linear dynamics analysis is next performed for each combination of the factor levels as defined in the appropriate row of the orthogonal matrix. The values of the objective function (the average residual velocity of the projectile) resulting from each of the 18 analyses are next displayed in Table 2 along

with the mean value of the objective function. It should be noted that the analysis 2 in Table 2, for which all four factors are set to level 2, corresponds to the analysis that has been carried out in Section III.2.

The mean values of the objective function associated with each of the three levels of each of the four factors are next calculated. This is done by averaging the values of the objective function associated with a specific level of a given factor. The results of this calculation are given in Table 3. The effect of a level of a factor is then defined as the deviation it causes from the overall mean value and is thus obtained by subtracting the overall mean value from the mean value associated with the particular level of that factor. This process of estimating the effect of factor levels is generally referred to as the "*Analysis of Means*" (ANOM). The ANOM allows determination of the main effect of each factor. However, using this procedure it is not possible to identify the possible interactions between the factors. In other words, the ANOM is based on the principle of linear superposition according to which the system response η (the objective function in the present case) is given by:

$$\eta = \textit{overall mean} + \Sigma\ \textit{(factor effect)} + \textit{error} \qquad \textbf{(9)}$$

where *error* denotes the error associated with the linear superposition approximation.

To obtain a more accurate indication of the relative importance of the factors and their interactions, the "*Analysis of Variance*" (ANOVA) is used. The ANOVA allows determination of the contribution of each factor to the total variation from the overall mean value. This contribution is computed in the following way: First, the sum of squares of the differences between the mean value associated with each level of a given factor and the overall mean value of the objective function is calculated. The percentage, by which this sum for a given factor contributes to the cumulative sum for all factors, is then used as measure of the relative importance of that factor.

The ANOVA also allows estimation of the error associated with the linear superposition assumption. The method used for the error estimation generally depends on the number of factors and factor levels as well as on the type of the orthogonal matrix used in the statistical sensitivity analysis. The method described below which is

generally referred to as the "*sum of squares*" method is used in the present work. According to this method, the sum of squares due to the error, SS_{error}, is calculated as:

$$SS_{error} = SS_{grand} - SS_{mean} - SS_{factors} \quad \textbf{(10)}$$

where SS_{grand} is the sum of the squares of the objective function values for all the analyses, SS_{mean} value is equal to the overall mean squared multiplied by the number of analyses and $SS_{factors}$ is equal to the sum of squares of the differences between the mean value of the objective function associated with each level of all the factors and the overall mean value of the objective function. Each quantity in Eq. (10) is associated with a specific number of degrees of freedom. The number of degrees of freedom for the grand total sum of squares, DOF_{grand}, is equal to the number of analyses (i.e. the number of rows in the orthogonal matrix). The number of degrees of freedom associated with the mean value, DOF_{mean}, , is one. The number of degrees of freedom for each factor, DOF_{factor}, is one less (= 2) than the number of levels for that factor (= 3). The number of degrees of freedom for the error can hence be calculated as:

$$DOF_{error} = DOF_{grand} - 1 - \Sigma(DOF_{factor}) \quad \textbf{(11)}$$

For Eq. (10) to be applicable, the number of degrees of freedom for the error must be greater than zero. If the number of degrees of freedom for the error is zero, a different method must be used to estimate the linear superposition error. An approximate estimate of the sum of the squares due to the error can be obtained using the sum of squares and the corresponding number of degrees of freedom associated with the half of the factors with the lowest mean square. In the present work, nine degrees of freedom for the error were found.

Once the sum of squares due to the error and the corresponding number of degrees of freedom for the error have been calculated, the error variance, VAR_{error}, and the variance ratio, F, can be computed as:

$$VAR_{error} = SS_{error}/DOF_{error} \quad \textbf{(12)}$$

and

$$F = (MEAN_{factor})^2 / VAR_{error} \quad \textbf{(13)}$$

where $MEAN_{factor}$ is a mean value of the deviations of the objective function for a given factor. The varaince ratio, F, is used to quantify the relative magnitude of the effect of each factor. A value of F less than one normally implies that the effect of the corresponding given factor is smaller than the error associated with the linear superposition approximation and hence can be ignored. A value of F above four, on the other hand, generally suggests that the effect of the factor at hand is significant.

Since the values for all four factors used in the present work are less than 4, Table 3, it can be concluded that variations in the material model parameters within one positive or negative standard deviation do not significantly affect the results of the computational analysis of the ballistic performance of the optimal 2_T hybrid armor. In other words, the 2_T design remains the optimal one even after an account is taken for the uncertainty in the values of the material parameters for the MWCNT-reinforced poly-vinyl-ester-epoxy matrix mats. In addition, the results shown in Table 3 indicate that Factor C (the failure initiation stresses) and Factor D (fracture energies) are statistically most significant. This finding is consistent with the fact that the main projectile defeat mechanism in the present case is absorption of the projectiles kinetic energy which is mainly controlled by the materials failure model.

III.4 The Effect of the MWCNT-reinforcement Aspect Ratio

The material model for the MWCNT-reinforced poly-vinyl-ester-epoxy matrix mats developed in our previous work [1], was based on a combination of the atomic-level calculations of the mechanical properties of the "*effective reinforcements*" (MWCNTs + the surrounding polymer matrix with an altered conformation) with a micro-mechanics approach for the determination of the continuum-type homogenized-material mechanical properties of the MWCNT-reinforced polymer matrix composite. During the atomic-level calculations, the MWCNT's are treated as being infinitely long due to the use of a unit-cell periodic-boundary approach. The effect of MWCNT aspect ratio was then added within the micro-mechanics approach but only for the calculations of the composite material stiffness properties. The effect of the MWCNT aspect ratio on the strength and failure resistance of the material in question was not accounted for. Since, in general, the strength and the failure properties of the

discontinuous-fiber reinforced materials, as is the present case, can be affected by the reinforcement aspect ratio, the sensitivity of the model predictions discussed in Section III.2 to the MWCNT aspect ratio is presented in this section.

A review of the literature (e.g. [34]) reveals that the effect of the reinforcement aspect ratio in short-fiber reinforced composites can be generally summarized as follows:

(a) For unidirectionally-oriented short-fiber composites, the composite strength in the fiber direction increases with an increase in the aspect ratio from its lower-bound value associated with the spherical reinforcements to a nearly constant high-aspect ratio value;

(b) The short-fiber high aspect ratio strength value is lower (typically by 15-25 %) than the corresponding continuous fiber strength value at the same reinforcement volume fraction;

(c) The critical (minimal) value of the reinforcement aspect ratio beyond which the composite strength is essentially independent of the reinforcement aspect ratio is defined from the condition that the force required to cause tensile failure of a fiber ($\pi r^2 \sigma_f$, r = the fiber radius and σ_f = the fiber tensile strength) is lower than the force required to cause shear failure at the reinforcement/matrix interface or in the matrix ($\pi r^2 L \tau_m$, L = the fiber length and τ_m = the shear strength of the matrix or the shear strength of fiber/matrix interface); and

(d) The critical reinforcement aspect ratio for strength in short-fiber reinforced composites is typically 5 to 10 times larger than its counterpart for the Young's modulus of the same type of composite material.

The atomic simulation results obtained in our previous work [5] revealed that the effective-reinforcement/matrix interfacial failure is controlled by the poly-vinyl-ester-epoxy matrix shear. Based on this observation and using typical values for the fracture stress of a MWCNT (900-1200 MPa) and a typical value for the shear strength of the poly-vinyl-ester-epoxy (20-30 MPa), the minimal critical strength aspect ratio for the effective reinforcement 15-30 is obtained. Since this value is relatively small when compared with the average aspect ratio (>100) of the MWCNT-reinforcement used in

our ongoing experimental work, it appears that the assumption made in our previous work [1], that the strength of the MWCNT-reinforced poly-vinyl-ester-epoxy in the direction of the reinforcements can be approximately set to 80% of that for the continuous fiber reinforced composites, appears justified.

A review of the literature (e.g. [34]) shows that the reinforcement aspect ratio has only a weak effect on the toughness of the short-fiber reinforced composites. Based on the finding it is assumed in the present work that the reinforcement aspect ratio has no effect on the failure parameters of the 3WCNT-reinforced poly-vinyl-ester-epoxy material. This can be justified as follows:

(a) The tensile failure stress, σ_{ij}^{*}, controlling the initiation of failure are primarily governed by the strength of the functionalizing covalent bonds and the extent of entanglement of the polymer segments (covalently bonded to the nanotube outer wall) with the polymer matrix. These two factors are controlled by the extent of covalent functionalization of the nanotube outer walls and the length of the covalently attached polymer chain segments and not by the nanotube length; and

(b) The maximum crack strains are primarily governed by the extent of the fiber pull-out before either the functionalizing covalent bonds break or the covalently attached polymer chain segments become disentangled from the polymer matrix. Again, these phenomena are only weakly affected by the nanotube length/aspect ratio.

IV. SUMMARY AND CONCLUSIONS

Based on the results obtained in the present work, the following summary and main conclusions can be made:

1. The material model for an E-glass reinforced poly-vinyl-ester-epoxy matrix composite proposed in our previous work [1] realistically accounts for the behavior of this material when subjected to high deformation rates and high deformations during a projectile impact.

2. Both the location and the thickness of MWCNT-reinforced poly-vinyl-ester-epoxy matrix composite mats within a hybrid armor based on E-glass reinforced poly-vinyl-ester-epoxy composite laminas affect the ballistic performance of the armor.

3. The optimal hybrid armor design is associated with thicker (100μm thick) MWCNT-reinforced poly-vinyl-ester-epoxy matrix composite mats placed near the front face of the armor.

4. The use of the statistical sensitivity analysis (ANOVA) revealed that the computational results which were used to identify the optimal armor design are not very sensitive to the identified uncertainty in the material model parameters.

V. ACKNOWLEDGEMENTS

The material presented in this paper is based on work supported by the Naval Research Office ender the Grant Number N00014-05-1-0844, by the U.S. Army/Clemson University Cooperative Agreement Number W911NF-04-2-0024 and by the U.S. Army Grant Number DAAD19-01-1-0661. The authors are indebted to Dr. Tom Juska of the Naval Research Laboratory and to Drs. Walter Roy, Bryan Cheeseman and Fred Stanton from the Army Research Laboratory.

REFERENCES

1. **M. Grujicic. Y.-P. Sun and K. L. Koudela, "Micro-mechanics Based Derivation of the Materials Constitutive Relations for Carbon Nanotube Reinforced Poly-Vinyl-Ester-Epoxy Based Composites,"** *J. Mater. Sci.*, **submitted for publication, April 2006.**
2. **U.S. Military Department of Defense Specification, MIL-A-12560H95, July 1991.**
3. **K. Williams and K. Poon, "A Numerical Analysis of the Effect of Surrogate Anti-Tank Mine Blasts on the M113,"** *DREV TM-2000-007*, **DRDC, Valcartier, Quebec, Canada, 2000.**
4. **M. Grujicic, B. Pandurangan, K. L. Koudela and B. A. Cheeseman, "A Computational Analysis of the Ballistic Performance of Light-Weight Hybrid-Composite Armor,"** *Appl. Surf. Sci.*, **accepted for publication, January 2006.**
5. **M. Grujicic. Y.-P. Sun and K. L. Koudela, "The Effect of Covalent Functionalization of Carbon Nanotube Reinforcements on the Atomic-Level Mechanical Properties of Poly-Vinyl-Ester-Epoxy,"** *Appl. Surf. Sci.,* **submitted for publication, December 2005.**
6. **J. Zhu, J. Kim, H. Peng, J. L. Margrave, V. N. Khabashesku and E. V. Barrera,** *Nano Lett.*, **3 (2003) 1107.**
7. **B. Ashrafi and P. Hubert, "Modeling the Elastic Properties of Carbon Nanotube Arrays/Polymer Composites,"** *Composites Science and Technology*, **66 (2006) 387.**
8. **O. Lourie and H. D. Wagner,** *J. Mater. Res.*, **13 (1998) 2418.**
9. **D. A. Walters, L. M. Ericson, M. J. Casavant, J. Liu, D. T. Colbert, K. A. Smith and R. E. Smalley,** *Appl. Phys. Lett.*, **74 (1999) 3803.**
10. **R. Andrews, D. Jacques, A. M. Rao, T. Rantell, F. Derbyshire, Y. Chen, J. Chen and R. C. Haddon,** *Appl. Phys. Lett.*, **75 (1999) 1329.**
11. **A. A. Mamedov, N. A. Kotov, M. Prato, D. M. Guldi, J. P. Wicksted and A. Hirsch,** *Nat. Mater.*, **1 (2002) 190.**
12. **J. P. Salvetat, G. A. D. Briggs, J. M. Bonard, R. R. Bacsa, A. J. Kulik, T. Stockli, N. A. Burnham and L. Forro,** *Phys. Rev. Lett.*, **82 (1999) 944.**
13. **J. Chen , A. M. Rao, S. Lyuksyutov, M. E. Itkis, M. A. Hamon, H. Hu, R. W. Cohn, P. C. Eklund, D. T. Colbert, R. E. Smalley and R. C. Haddon** *J. Phys. Chem.*, **B 105 (2001) 2525.**
14. **S. J. V. Frankland, A. Caglar, D. W. Brenner and M. Griebel,** *J. Phys. Chem.*, **B 106 (2002) 3046.**
15. **P. C. P. Watts, W. K. Hsu, G. Z. Chen, D. J. Fray, H. W. Kroto and D. R. M. Walton,** *J. Mater. Chem.*, **11 (2001) 2482.**
16. **A. Thess,** *Science*, **273 (1996) 483.**

17. **A. Kis, G. Csanyi, J-P. Salvetat, T-N. Lee, E. Couteau, A. J. Kulik, W. Benoit, J. Brugger and L. Forro,** *Nat. Mater.*, **3 (2004) 153.**

18. **A. B. Dalton, S. Collins, E. Munoz, J. M. Razal, V. H. Ebron, J. P. Ferraris, J. N. Coleman, B. G. Kim and R. H. Baughman,** *Nature*, **423 (2003) 703.**

19. **H. W. Zhu, C. L. Xu, D. H. Wu, B. Q. Wei, R. Vajtai R and P. M. Ajayan,** *Science*, **296 (2002) 884.**

20. **M. Grujicic, Y.-P. Sun and K. L. Koudela,** *Unpublished Work*, **Clemson University, 2006.**

21. **M. Grujicic, G. Cao and W. N. Roy,** *Appl. Surf. Sci.*, **227 (2004) 349.**

22. **M. Grujicic, G. Cao and W. N. Roy,** *J. Mater. Sci.*, **39 (2004) 2315.**

23. **AUTODYN-2D and 3D, Version 6.1,** *User Documentation,* **Century Dynamics Inc., 2006.**

24. **M. Grujicic, B. Pandurangan and B. A. Cheeseman,** *Shock and Vib.,* **13 (2006) 41.**

25. **G. R. Johnson and W. H. Cook**, "**A Constitutive Model and Data for Metals Subjected to Large Strains, High Strain Rates and High Temperatures**," *Proceedings of the 7th International Symposium on Ballistics,* **1983**.

26. **R. A. Clegg, C. J. Hayhurst, J. G. Leahy and M. Deutekon, "Application of a Coupled Anisotropic Material Model to High Velocity Impact Response of Composite Textile Armor," 18th** *International Symposium on Ballistics*, **San Antonio, Texas, 15-19 November, 1999, 791-798.**

27. **C. E. Anderson, P. A. Cox, G. R. Johnson and P. J. Maudlin,** *Comput. Mech.*, **15, (1994) 201.**

28. **M. Grujicic, B. Pandurangan, U. Zecevic, K. L. Koudela and B. A. Cheeseman, " Ballistic Performance of Alumina/S-2 Glass Fiber-Reinforced Polymer-Matrix Composite Hybrid Light-Weight Armor Against Armor Piercing (AP) and Non-AP Projectiles,"** *Appl. Surf. Sci.*, **submitted for publication, February 2006.**

29. **Gruneisen,** *Handbuch der Physik,* **Springer-Verlag, Berlin, 10, 1926.**

30. **W. Riedel, D. M. White, R. A. Clegg and W. Harwick,** *Advanced Material Damage Models for Numerical Simulation Codes*, **EMI-Report No. I 75/03, ESA CR (P) 4379, October 2003.**

31. **M. S. Phadke**, "*Quality Engineering Using Robust Design,*" **Prentice Hall, Englewood Cliffs, NJ, 1989.**

32. **D. C. Montgomery,** *Design and Analysis of Experiments*, **Wiley Publishers, August 2002.**

33. **P. J. Ross**, "*Taguchi Techniques for Quality Engineering: Loss Function, Orthogonal Experiments, Parameter and Tolerance Design*," **Second Edition, McGraw-Hill, New York, 1996.**

34. J. L. Kardos, "Critical Issues in Achieving Desirable Mechanical Properties for Short Fiber Composites," *Pure Appl. Chem.*, **57 (1985) 1651.**

Table 1. Statistical Sensitivity Analysis Factors and Levels Used in the Present Work

Factors	Levels		
	1	2	3
Stiffness (A)	0.88	1.0	1.12
Strength (B)	0.91	1.0	1.09
Failure Initiation Stresses (C)	0.87	1.0	1.13
Fracture Toughness (D)	0.93	1.0	1.07

Table 2. L_{18} (3^4) Orthogonal Matrix Used in the Statistical Sensitivity Analysis

Analysis Number	Levels				FSP Residual Velocity (m/s)
	Factor A	Factor B	Factor C	Factor D	
1	1	1	1	1	127.19
2	2	2	2	2	134.10
3	3	3	3	3	133.96
4	1	1	2	2	130.10
5	2	2	3	3	136.62
6	3	3	1	1	128.66
7	1	2	1	3	136.70
8	2	3	2	1	133.22
9	3	1	3	2	134.66
10	1	3	3	2	138.11
11	2	1	1	3	127.47
12	3	2	2	1	129.41
13	1	2	3	1	131.68
14	2	3	1	2	133.33
15	3	1	2	3	134.29
16	1	3	2	3	136.00
17	2	1	3	1	131.95
18	3	2	1	2	128.84
Overall Mean of the FSP Residual Velocity, (m/s)					132.57

Table 3 Statistical Sensitivity Analysis of the Optimal Design of the 2_T Hybrid Armor

Factor	Difference From Mean, (m/s)			Sum of Squares $(m/s)^2$	Percent of Sum of Squares	Number of D.O.F	Variance Ratio F
	Level 1	Level 2	Level 3				
A	0.7250	0.2100	-0.9350	1.4439	6.29	2	0.489
B	-1.6283	0.3200	1.3083	4.4656	19.49	2	1.511
C	-2.2067	0.2817	1.9250	8.6543	37.73	2	2.930
D	-2.2200	0.6183	1.6017	7.8761	34.34	2	2.6664
Error	N/A			0.4923	2.15	9	N/A
	Total			22.932	100.00	N/A	N/A

FIGURE CAPTIONS

Figure 1 A schematic of the projectile/armor impact analyzed in the present work.

Figure 2 Various hybrid-armor design configurations analyzed in the present work.

Figure 3 Temporal evolution of a 0.50 caliber FSP velocity during the impact with a 25.4 mm-thick all E-glass continuous-fiber reinforced poly-vinyl-ester-epoxy matrix composite armor.

Figure 4 Experimental (a) and computational (b) material distribution/damage results pertaining to the impact of a 0.50 caliber FSP with a 25.4 mm-thick all E-glass continuous-fiber reinforced poly-vinyl-ester-epoxy matrix composite armor. Initial projectile velocity, 605 m/s.

Figure 5 Temporal evolution of the 0.30 caliber projectile velocity for various 12.7 mm-thick hybrid armor configurations. Please refer to the text for the explanation of symbols.

Figure 6. A comparison of the material deformation/failure status plots for the 2_T and 2_B hybrid armors at the same projectile post-impact time of 0.04ms. It should be noted that the axis in this figure is rotated by 90 degrees relative to those used in Figures 1, 2 and 4.

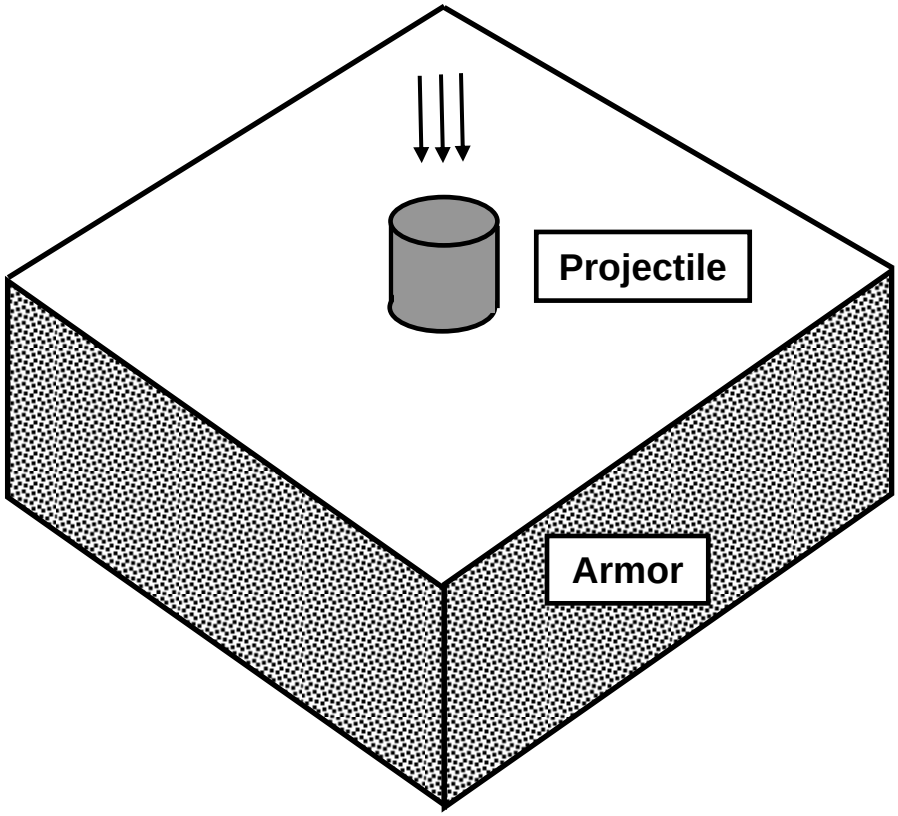

Figure 1. A schematic of the projectile/armor impact analyzed in the present work.

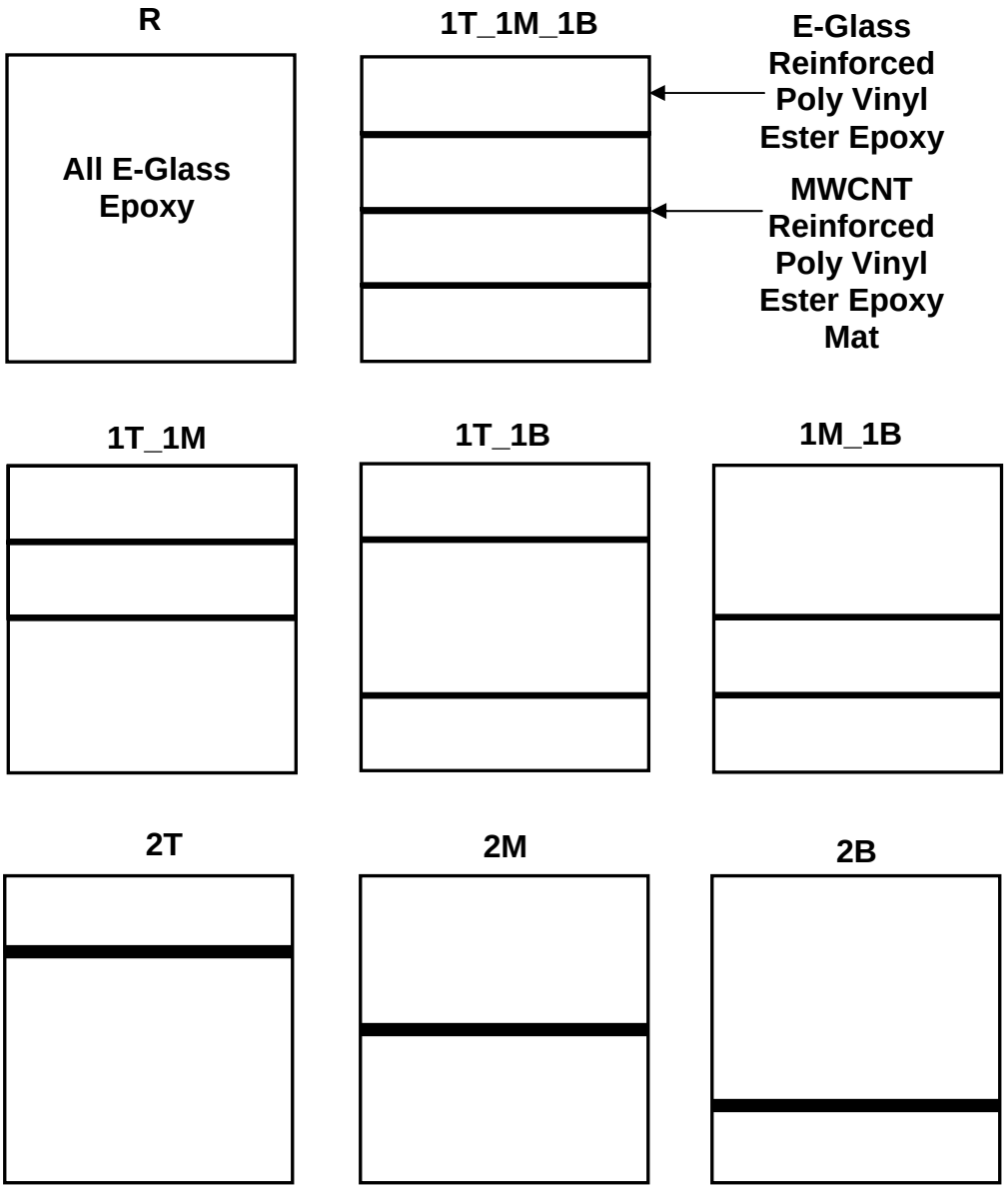

Figure 2 Various hybrid-armor design configurations analyzed in the present work.

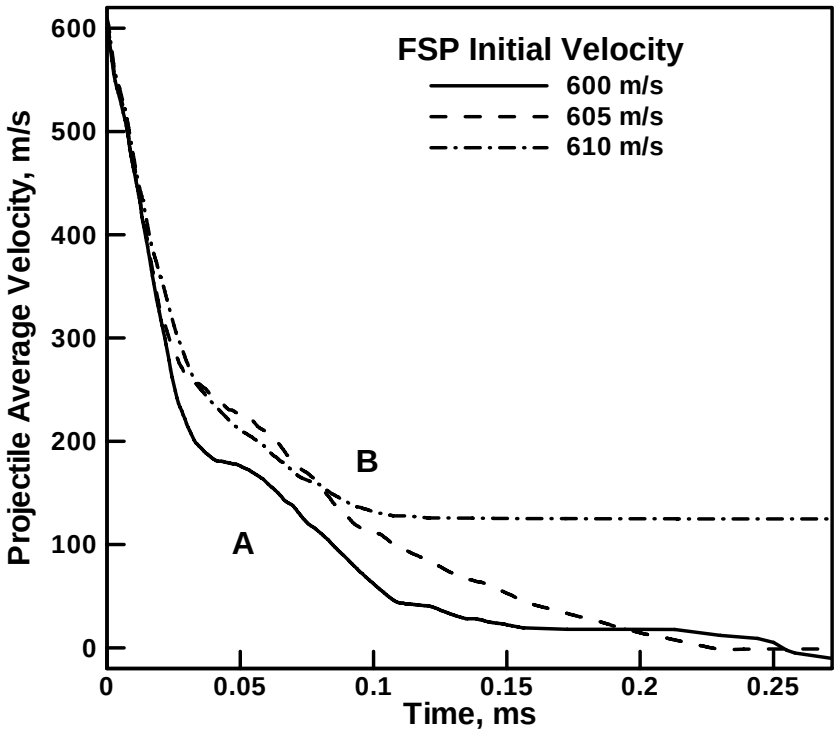

Figure 3 Temporal evolution of a 0.50 caliber FSP velocity during the impact with a 25.4 mm-thick all E-glass continuous fiber-reinforced poly-vinyl-ester-epoxy matrix composite armor.

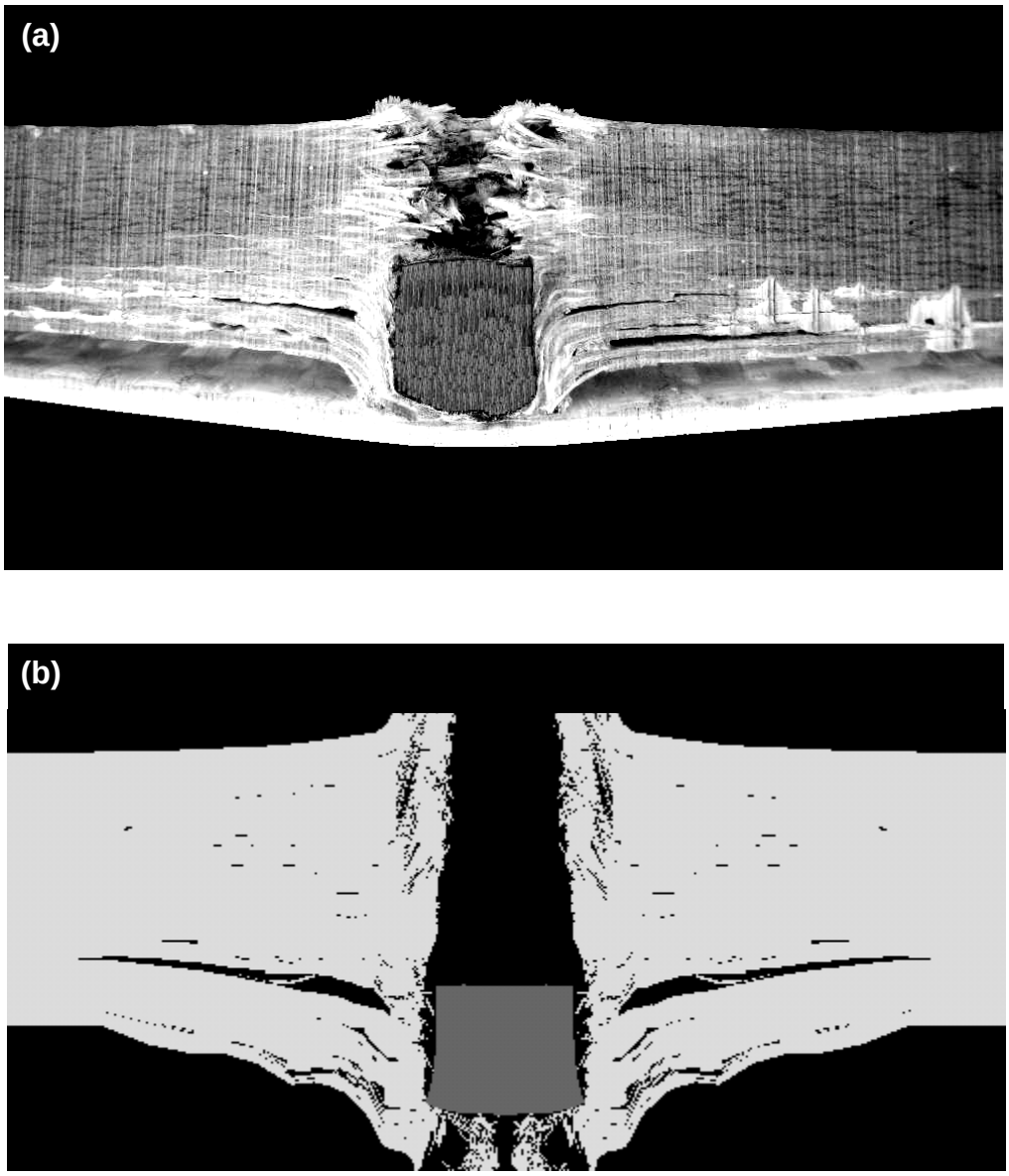

Figure 4 Experimental (a) and computational (b) material distribution/damage results pertaining to the impact of a 0.50 caliber FSP with a 25.4 mm-thick all E-glass continuous-fiber reinforced poly-vinyl-ester-epoxy matrix composite armor. Initial projectile velocity, 605 m/s.

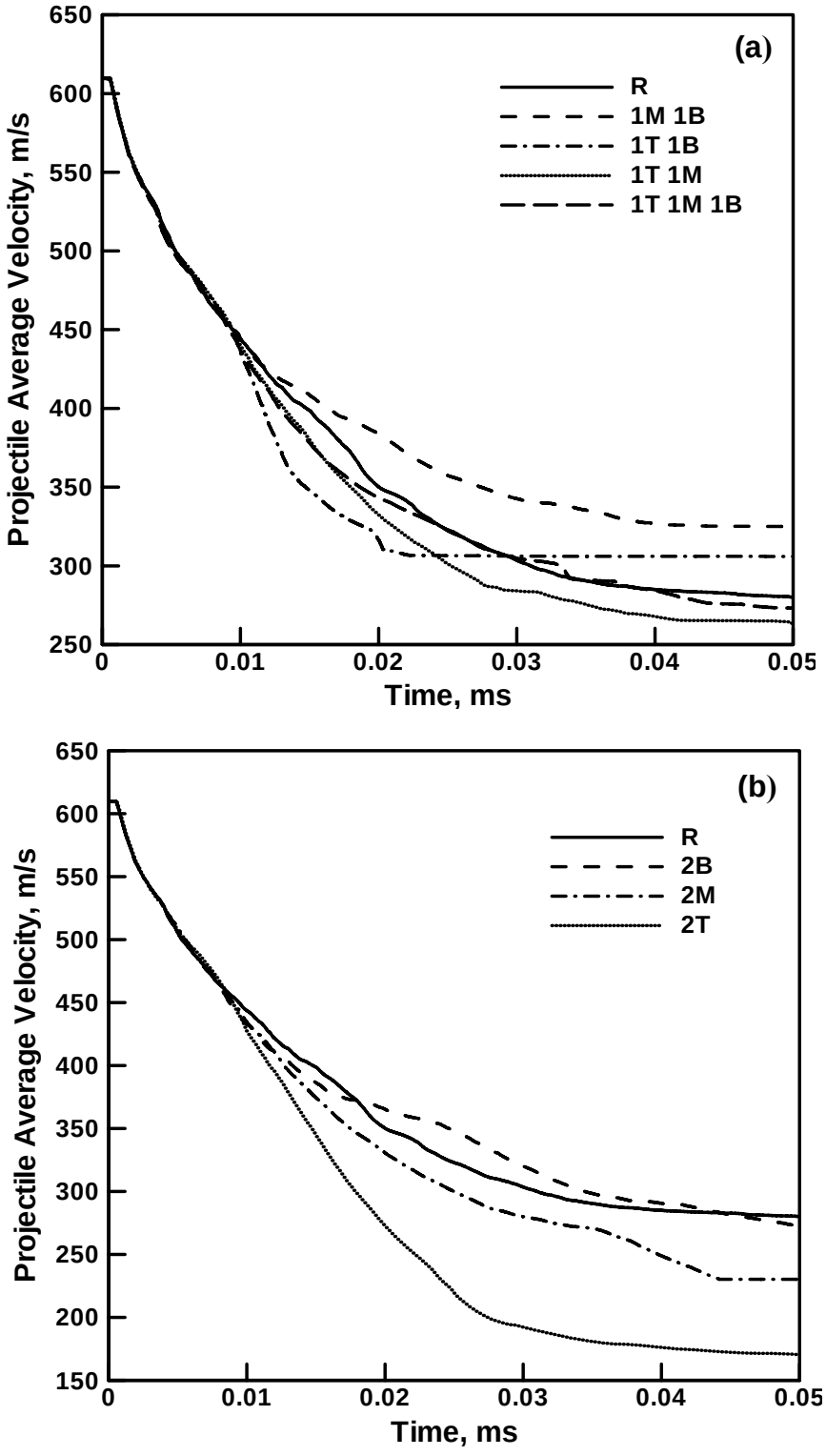

Figure 5 Temporal evolution of the 0.30 caliber projectile velocity for various 12.7 mm-thick hybrid armor configurations. Please refer to the text for the explanation of symbols.

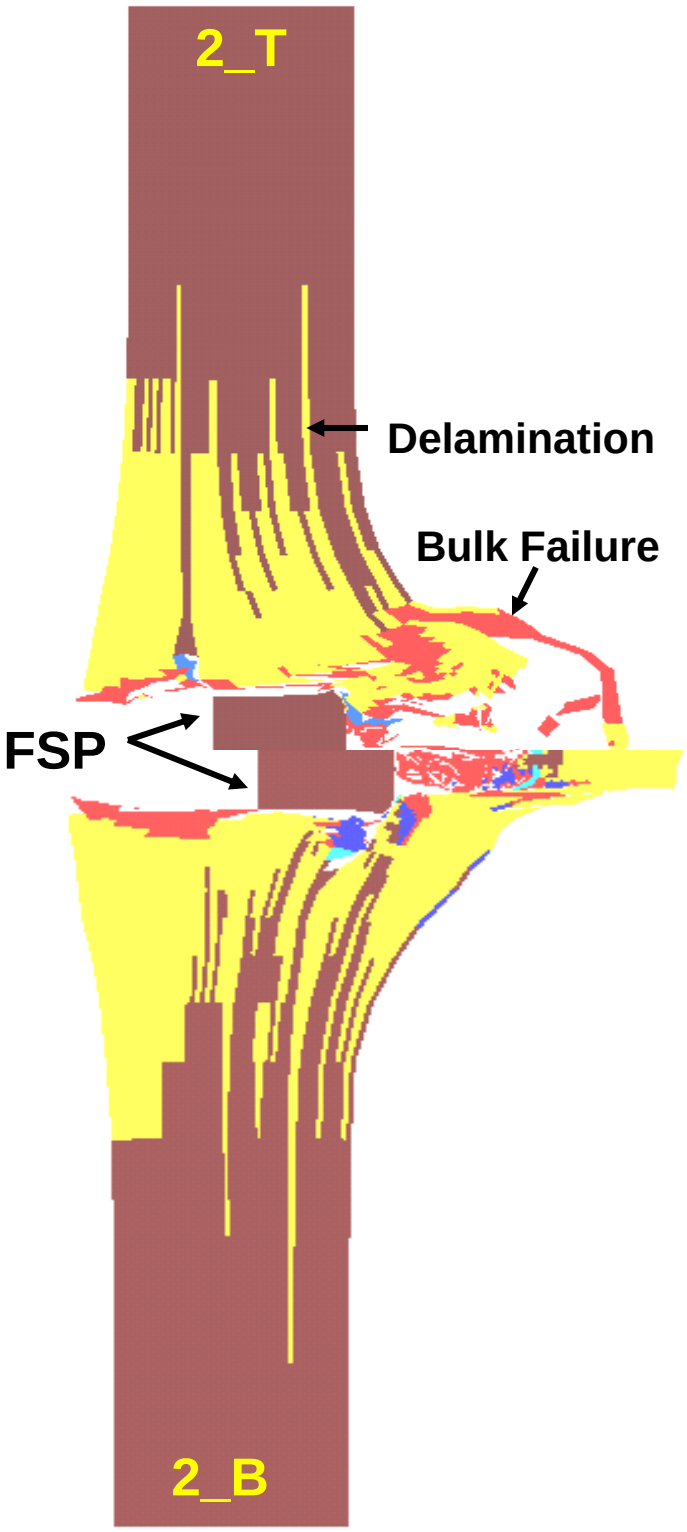

Figure 6. A comparison of the material deformation/failure status plots for the 2_T and 2_B hybrid armors at the same projectile post-impact time of 0.04ms. It should be noted that the axis in this figure is rotated by 90 degrees relative to those used in Figures 1, 2 and 4.